Impact Factor (SJIF): 6.092 E-ISSN: 2583-1615

International Journal of Research in Academic World

Received: 02/April/2024 IJRAW: 2024; 3(5):22-29 Accepted: 08/May/2024

Collaboration of Manufactured $Pb_2Cd_4Sr_2O_{10}$ with Solar Energy to Remove Erythrocine B from Water

[1]Dushyant Kumar Prajapati, [2]Jinesh Menaria, [3]Jeevan Kunwar Chouhan, [4]Tejveer Singh Tanwer and *[5]Shipra Bhardwaj

[1, 2, 3, 4, *5]Department of Chemistry, Government Meera Girls College, Mohan Lal Sukhadia University, Udaipur, Rajasthan, India.

Abstract

In search of remedy to water pollution, a new nanomaterial $Pb_2Cd_4Sr_2O_{10}$ is synthesized by co-precipitation method and calcined. It is then characterized by various analytical methods like Fe-SEM, XRD, XPS, EDX etc. Band gap of the material is calculated to be 5.6 eV. This is then used for degradation of Erythrosine B in solar light and is observed to degrade it up to 98% in 60 minutes of exposure. Study suggests that reaction follows pseudo first order kinetic law. Maximum degradation conditions are extracted by varying the affecting factors and the rate constant obtained is 4.007 x 10^{-4} sec^{-1}. Scavenger study suggests participation of •OH free radicals. Recycling experiment states that the photocatalyst can be used again up to five cycles without any loss in its efficiency. End products are ascertained by laboratory tests. A mechanism is also proposed.

Keywords: Photocatalysis, characterization, photodegradation, quaternary metal oxide, ISO propyl alcohol

1. Introduction

Water pollution is the worst problem amongst all the environmental issues and is affecting life acutely due to urbanization, industrialization and other factors. Treatment of such water through various means thus becomes mandatory. Different method like filtration, coagulation, chemical processes etc. were therefore employed for this purpose but were found effective up to a certain limit. Gradually scientists were able to explore the advance oxidation process (AOP) and use of solar energy. Yang *et al.* [1] tried to use solar radiation to turn water into hydrogen fuel since 1970s. Xu *et al.* [2] stated that photocatalysis is a green technique that converts light energy into chemical energy. TiO_2 photocatalysis played a critical role in energy and environmental applications, and researches brought attention to the need for such materials [3]. Wenderich *et al.* [4] studied the impact on photocatalytic activity of particle size distributions, and metal oxidation states of semiconductors and metals during photodeposition.

Surface of ZnO-based photocatalyst was modified with Cu^{2+} and flame spray pyrolysis. The prepared material was able to neutralize pathogens at exposure to visible light[5]. Cu^{2+} ion addition enhanced light absorption in ZnO by promoting interfacial charge transfer. ZnO structure in the form of sheets and flowers was successfully synthesized by Xie *et al.* [6] via hydrothermal synthesis; 2 µm-diameter flower-like nanostructures in the form of sheets were produced by extending the reaction time. The rate constants (ranging from 1.17 × 10^{-2} to 3.42 × 10^{-2} min^{-1}) obtained from the photodegradation demonstrated pseudo-first-order kinetics.

Co-precipitation was used to produce Mn, Co, and Mn-Co-doped TiO_2 semiconducting particles by Kiriakidis *et al.* [7]. Under visible light irradiation, these doped TiO_2 materials were used as visible light photocatalysts for degradation of methylene blue. Using a co-precipitation and calcination method, Wang *et al.* [8] prepared rambutan-fruit-like hierarchical microspheres of $MnCo_2O_4$ with a large surface area of 155 m^2 g^{-1}. The adsorption kinetics of methyl orange (MO) on it revealed pseudo-second-order model with an enthalpy (ΔH#) of 9.30 kJ mol^{-1} and an activation energy (Ea) of 5.71 ± 0.056 kJ mol^{-1}.

Microcrystalline $ABi_2Nb_2O_9$ (A=Sr, Ba) photocatalysts were successfully synthesized by Wu *et al.* [9] employing a citrate complex method. Band gaps of 3.34-3.54 eV was found in tetragonal $BaBi_2Nb_2O_9$ and orthorhombic $SrBi_2Nb_2O_9$ respectively. $SrBi_2Nb_2O_9$ performed better than $BaBi_2Nb_2O_9$ in UV light-induced photocatalytic redox reactions of methyl orange, indicating the impact of crystallinities, BET surface areas, and crystal morphologies on the photocatalytic performance.

Tetracycline (TC) molecules were broken down with remarkable efficiency by the ZnO/NiO/g-C_3N_4 photocatalysts when exposed to visible light and reached 91.49%disintegration rate in 60 minutes. The composite also demonstrated remarkable stability, showing 88.76% TC degradation efficiency even after three cycles [10]. The effects of the La/Al ratio and the calcination temperature on

*Corresponding Author: Shipra Bhardwaj

photocatalytic activity were investigated by Elhalil *et al.* [11] they also studied the degradation of caffeine under UV light. Nanomaterial Ag-ZnO-$La_2O_2CO_3$ was synthesized as effective photocatalyst to break down such pharmaceutical contaminants. Zhang *et al.* [12] synthesized Ag_2O/g-C_3N_4/Fe_3O_4 nanocomposites which were found environmentally benign. Under visible light, these nanocomposites showed stability and effectiveness in Rhodamine B (RhB) photodegradation. 10 mg/L RhB was destroyed under 500 W of visible light exposure for 60 minutes, by 98.3%. Kinetics of photodegradation and the possible mechanism were also studied.

Cu_2O/ZnO/Ag_3PO_4, a ternary composite with p-n heterojunctions and a predicted band gap of 2.15 eV, was synthesized by Taddesse *et al.* [13]. This heterojunction was found to affect the band gap of ZnO (3.18 eV). The composite's photocatalytic degradation efficiency under visible light was higher than that of its single and binary equivalents, with higher rates of 81.1% for methyl orange (MO) and 78.2% for textile effluent.

Nanocomposite using SiO_2/TiO_2 nanoparticles coating on the Fe_3O_4 core and the $PrVO_4$, were prepared by an ultrasonic-assisted co-precipitation method [14]. SEM examination revealed that the crystalline diameters of the prepared Fe_3O_4/SiO_2/TiO_2/$PrVO_4$ and Fe_3O_4/SiO_2/TiO_2/TiO_2 nanoparticles were 80-100 nm and 55-75 nm, respectively. The optimized sample showed efficient photocatalytic 55% degradation of rhodamine-B under visible light in 100 minutes. Gd-doped Cobalt Tin Oxide ($CoSnO_3$) nanocomposite was synthesized using two-step method, and the impact of calcination temperature on their photocatalytic activity was investigated by Muneer *et al.* [15]. The nanocomposite showed over 90% photo-degradation of methyl orange and methylene blue dyes. Using the combustion approach, nanostructures of the Quaternary metal oxide La_2-xBixCuO_4 with different amounts of Bi inclusion (x = 0, 0.01, 0.03, 0.06, 0.08) were prepared by Marzougui *et al.* [16]. These structures exhibited excellent efficiency in the degradation of malachite green in the presence of sun light. The degradation rates for x = 0, 0.01, 0.03, 0.06, and 0.08 were 64%, 68%, 75%, 89%, and 83% respectively after 240 minutes.

CeO_2/Co_3O_4 nanofibers and quaternary composites CeO_2/Co_3O_4/Ag/Ag_3PO_4 using the electrospinning technique were prepared and showed an impressive 92.5% degradation of methylene blue dye in 80 minutes under blue LED illumination [17]. Nanosized photocatalyst $BaO_3TiO.SrO_3TiO$ for degradation of Azure B was used by Nihalani *et al.* [18] in an ecofriendly manner. A kinetic study suggested the break down to follow pseudo first order kinetic law. The nanocomposite doped with 0.3% Nd (Nd-ZnO-GO) was synthesized through co-precipitation and exhibited good efficiency in degrading organic pollutants [19]. It also showed a significant reduction in total organic carbon (TOC) levels, with a removal rate of 76% and minimizing the formation of harmful by-products. Furthermore, the nanocomposite maintained its stability and reused multiple times, with a degradation efficiency of 83.0% even after five cycles.

Nitrogen and palladium-co-doped TiO_2 was synthesized by a modified sol-gel technique, and its efficacy in degrading natural organic matter (NOM) under simulated solar radiation was assessed [20]. The NOM in the hydrophobic, hydrophilic, and transphobic fractions showed remarkable breakdown rates of 96%, 38%, and 15%, respectively. This was attributed to the smaller crystalline size, higher surface area, and co-synergistic doping's effects on the TiO_2. Haw *et al.* [21] were able to prepare $CoFe_2O_4$-TiO_2 photocatalyst with magnetic $CoFe_2O_4$ nanoparticles adorning 3D urchin-like TiO_2 microparticles. The lower recombination rate of photoexcited charge carriers in the $CoFe_2O_4$-3D TiO_2 nanocomposites was found responsible for this superiority in photodegradation of methylene blue. Spinel cubic $CoMnCrO_4$ was prepared by Moradnia *et al.* [22] via sol-gel method. The crystallite size obtained was 14 nm. The study investigated the effects of amount of nanoparticles, initial dye levels etc. on dye degradation efficiency. Oh *et al.* [23] used a sonochemical method for synthesis of $LaNiSbWO_4$-G modified with polyaniline (PANI) that could effectively break down gallic acid and safranin-O (SO) in visible light ($\lambda > 420$ nm). The LNSWGP composite demonstrated an impressive rate of degradation, removing 84% of SO and 92% of gallic acid in just 180 minutes.

Otgonbayar *et al.* [24] prepared a quaternary nanocomposite utilizing a hydrothermal technique for combining the potent components of graphene-based $LaYAgO_4$, graphene, and TiO_2. After 48 hours, the ternary nanocomposite, which had a notably high concentration of $LaYAgO_4$, exhibited an amazing rise in photocatalytic activity, producing a staggering 12.27% more methanol. $CsTaWO_6$, a mesoporous quaternary oxide, was successfully synthesized utilizing evaporation-induced self-assembly by Weller *et al.* [25]. It exhibited remarkable catalytic properties in terms of producing hydrogen and dissolving water. Researchers were able to increase its surface area to 78 m^2 g^{-1} and improve its textural qualities by using both additives and a carbonization/oxidation process. It was observed that the material's photocatalytic activity is influenced by both pore diameter and surface area, which emphasizes the critical role that mesoporous shape plays in maximizing the material's potential for photocatalytic applications.

It was observed that there were fewer numbers of quaternary photocatalysts known and prepared and were less used for removal of pollutants from water. Synthesis of them through some easier path way is required too. Thus, synthesis of a new, cheaper and effective ternary photocatalyst is carried and is then used for removal of contaminants specially dyes, converting them into smaller and harmless fragments making water clean up to a considerable extend.

2. Experimental

2.1. Synthesis of $Pb_2Cd_4Sr_2O_{10}$ Photocatalyst

All the chemicals were of analytical grade (> 99%) and were used without further purification. Lead nitrate hexahydrate ($Pb(NO_3)_2.6H_2O$, Molechem Co., Ltd., 99%), Cadmium nitrate tetrahydrate, Strontium nitrate ($Cd(NO_3)_2 \cdot 4H_2O$, $Sr(NO_3)_2$, Merck Co., Ltd., 99.5%). Ethanol absolute (CH_3CH_2OH, 99.9%), and sodium hydroxide pellets (NaOH, 96%, Merck Co. Ltd.). erythrosine B dye, EDTA, ether, isopropyl alcohol, sulphuric acid, hydrochloric acid, etc. of CDH make were used.

2.2. Characterization

The prepared photocatalyst $Pb_2Cd_4Sr_2O_{10}$ was characterized by various analytical techniques. X-ray diffraction (XRD) pattern was recorded by a Panalytical X Pert Pro, X-ray diffractometer using Ni-filtered Cu Ka radiation at a scan range of 10/2h/80, at 10 kV and 80 mA for monochromatized Cu Ka (k = 1.5418 Å) radiation. Scanning electron microscopy (SEM) measurements were carried out on a Nova Nano FE-SEM 450 (FEI) scanning electron microscope to

investigate the morphology and surface roughness of samples. SEM imaging conditions with the composition analysis were done by energy dispersive X-ray. The HRTEM Hitachi H-7500, a high-resolution transmission electron microscope was used for structural analysis. The XPS spectra were carried out by Physical Electronics (Model-PHI 5000 Versa Probe III analysis). Fourier transform infrared (FT-IR) spectra were recorded on an FT-IR Spectrum 2 (Perkin Elmer) spectrophotometer in KBr pellets in the 400-4000 cm-1 range. UV-vis diffuse reflectance spectra (DRS) were measured using a UV-vis NIR spectrophotometer (Perkin Elmer, U.S.A.).

2.3. Photocatalytic Study

The photo-degradation of erythrosine B (EB) in an aqueous solution was monitored in order to estimate the photocatalytic activity of $Pb_2Cd_4Sr_2O_{10}$. The selection of EB was based on its high resistance to light deterioration and optical absorption on to metal oxide surfaces. In experiment, 50 mL of 1×10^{-5} M EB dye solution was taken in a beaker and 0.10 g of photocatalyst was added. pH of the solution was recorded by pH meter (Hena pen type). It was then exposed to a 250watt tungsten arc lamp. Intensity of the radiations was recorded by solarimeter and decrease in optical density (O.D.) was monitored on a UV-Vis spectrophotometer (CHINO) at Λ_{max} 520 nm. The Beer-Lambert relation was used to calculate the percentage of degradation. It was calculated by:

$$\text{Percent Degradation} = (Co - C)/Co\ X\ 100$$

Where C_o and C represent the initial concentration and final concentration of the dye at different time intervals, respectively.

3. Result and Discussion

3.1. Synthesis of $Pb_2Cd_4Sr_2O_{10}$ Photocatalyst

A solution containing metallic precursors is prepared using doubly distilled water, with each component at a concentration of 0.1 mol/L (lead nitrate, 3.31g, pH 7.5, cadmium nitrate, 3.08g, pH 6.7 and strontium chloride, 2.66g, pH 5.8). These filtered solutions are mixed and stirred using a magnetic stirrer at room temperature (25°C). A pre-standardized NaOH solution is added drop by drop until precipitation is complete. The precipitate is allowed to settle, filtered, thoroughly washed with distilled water and is tested for presence of impurities, elements and base. It is then dried in a microwave oven at 120°C, followed by grinding. The yield of the obtained white precipitate is 50.105 g. The powder is then calcined at 350°C in a muffle furnace for 5 hours, resulting in fine dark brown powder of $Pb_2Cd_4Sr_2O_{10}$. The yield then is 37.52g, with a product yield efficiency of 89.56%.

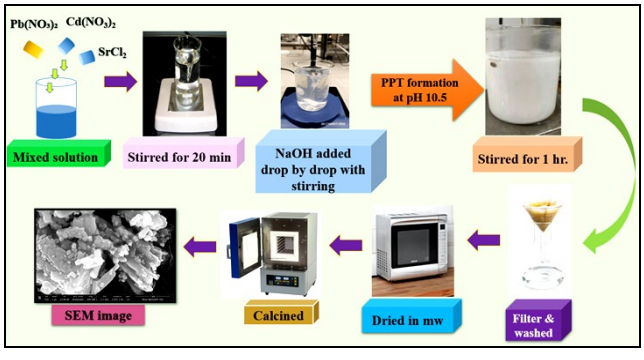

Fig 1: Flow chart of synthesis of $Pb_2Cd_4Sr_2O_{10}$ photocatalyst

3.2. X-Ray Diffraction Analysis

Using powder X-ray diffraction analysis, the crystallinity and phase purity of the prepared nanoparticles are verified. The data for calculation of crystal size are compiled in table 1 and various peaks of XRD are shown in figure 2.

Table 1: Crystal size of $Pb_2Cd_4Sr_2O_{10}$ photocatalyst

S. No.	Angle 2θ	FWHM	Crystal size (nm)	Average crystal size
1.	27.4348	0.1771	48.25	
2.	27.8633	0.1476	57.94	
3.	29.3283	0.1771	48.25	
4.	30.8726	0.2066	41.68	46.96 nm
5.	32.0329	0.3542	24.38	
6.	33.0161	0.1181	73.31	
7.	34.9720	0.2362	34.97	

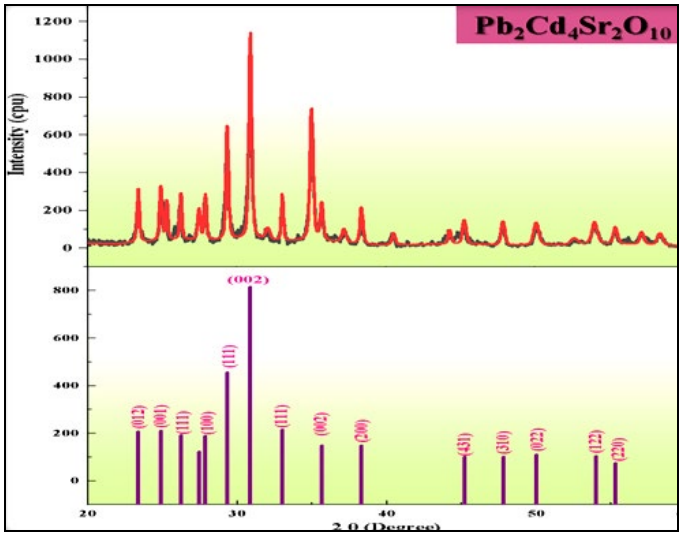

Fig 2: XRD pattern of $Pb_2Cd_4Sr_2O_{10}$ photocatalyst

High crystallinity and phase purity of the as-obtained photocatalyst is shown by the relatively narrow and sharp diffraction peaks. It shows a strong agreement with the typical XRD peaks of its predecessors. Diffraction peaks at angle values of 2θ = 26.2, 29.3, 30.8 and 55.3 are ascribed to the planes (111), (111), (002) and (220), showing the tetragonal phase of PbO_2 [26, 27]. The peaks at the diffraction angles of 23.3, 30.8, 33.0, 35. 8, 38.3 and 47.7 are attributed to (012) (002) (111) (002) (310) and (200) planes, respectively and are assigned to crystalline CdO in cubic phase. [28, 29] Peaks for SrO_2 appear at angles 24.8,45.2,35.0,50.0 and were assigned to the planes (001), (431), (002), and (220), respectively.[30,31] Strong and crisp diffraction peaks that fit well with the database indicate the rectangular crystalline structure and phase purity of nanoparticles. Other discernible peaks for contaminants are not observed.

$Pb_2Cd_4Sr_2O_{10}$ is found to have an average crystal size of 46.96 nm, as calculated by the Debye-Scherrer formula-

$$D = 0.9\lambda/\beta \cos\theta \qquad (1)$$

The full width at half maximum (FWHM) of the peaks at the diffracting angle is denoted by λ, where D is mean crystalline size of the prepared nanomaterial, λ is the wavelength of the X-ray photons, θ is Bragg angle, β is line broadening at FWHM.

3.3. FE-SEM Analysis and Elemental Mapping

FE-SEM analysis was carried out to examined the consistency of the nanoparticles and is shown in figure 3. In order to examine the morphology, the particle size range was evaluated and the composition of the samples was also determined by elemental mapping analysis (figure 4).

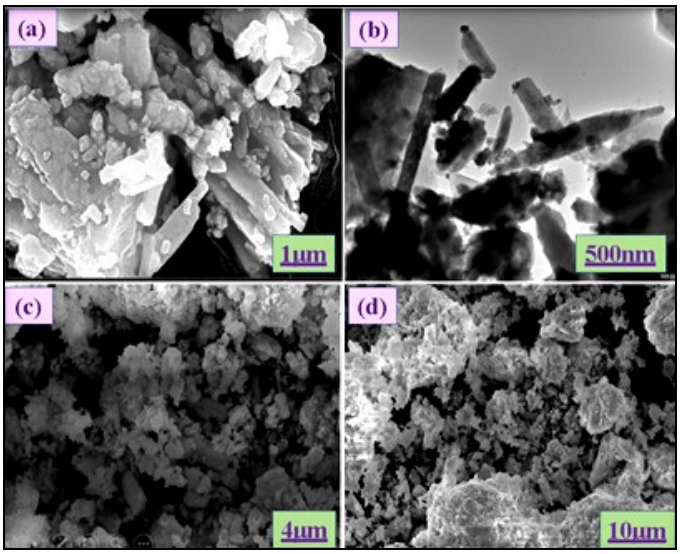

Fig 3: FE-SEM images of $Pb_2Cd_4Sr_2O_{10}$ photocatalyst

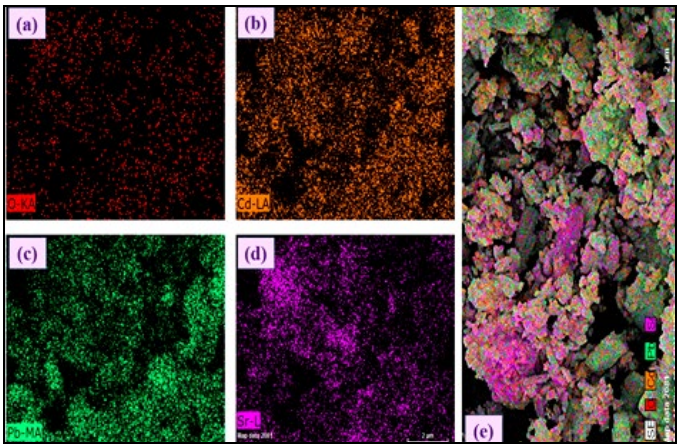

Fig 3: Elemental mapping of $Pb_2Cd_4Sr_2O_{10}$ photocatalyst

The particles are clumped together and have homogeneous cluster form. The image illustrates how the microscopic particles fuse together to form defined structure that resemble cubic strips or rods.

3.4. HRTEM Analysis

High-resolution transmission electron microscopy (HR-TEM) with the selected-area electron diffraction (SAED) pattern was used to examine the microstructural features in order to better understand the shape and size of $Pb_2Cd_4Sr_2O_{10}$ and is given in Figure 5.

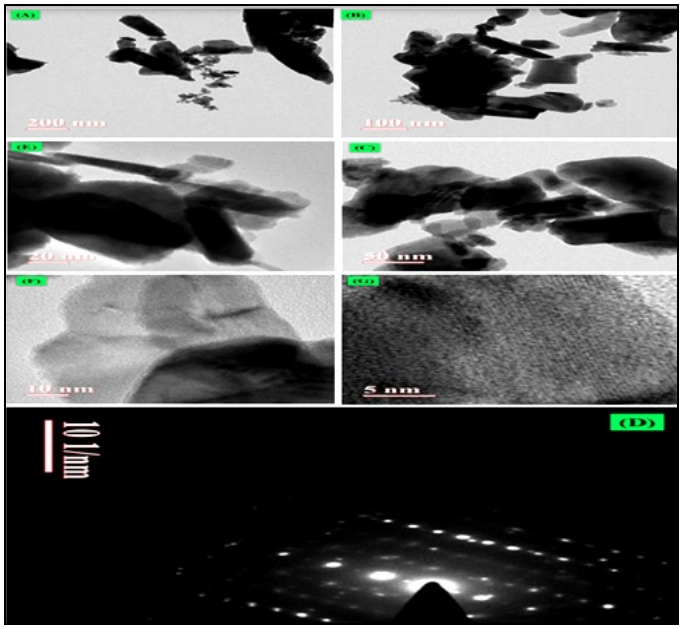

Fig 5: HRTEM images of $Pb_2Cd_4Sr_2O_{10}$ photocatalyst

D-spacing values of 0.212 nm and rectangular shape in two-dimensional sheet is seen in the lattice images. The diameter of crystallite measured by HR-TEM and those determined by powder XRD analysis appeared in good correlation. The particle sizes of the material varied from 50 nm to 200 nm.

3.5. EDX Analysis

The elemental composition and purity in the nanocomposite are assessed by the EDX analysis and is shown in figure 6.

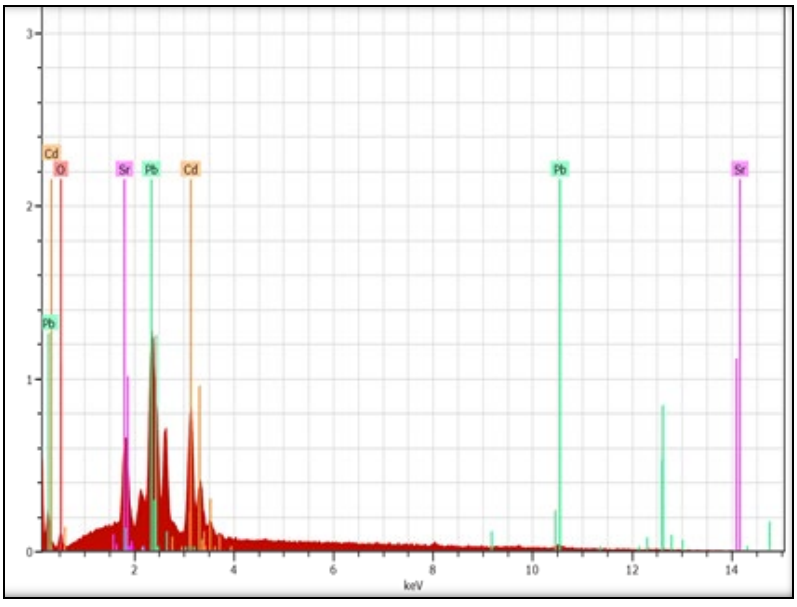

Fig 6: EDX spectra of $Pb_2Cd_4Sr_2O_{10}$ photocatalyst

Dispersive X-ray energy analysis graph shows the presence of Pb, Cd, Sr and O elements in the nanocomposite with ratio of 2.0:4.0:2.0:10.49 suggesting the empirical formula to be $Pb_2Cd_4Sr_2O_{10}$. The EDX spectra makes it clear that the nanocomposite material does not have any added impurities. A rectangular strip-like crystal structure was seen indicating the development of mixed phases in the XRD spectra that corroborate with the EDX findings. Further, the results indicate the purity of the phase in the composite.

3.6. XPS Analysis

XPS helps in figuring out the atomic composition and chemical identities of the composite. The presence of PbO_2, CdO, and SrO in the photocatalyst is confirmed by the spectra of the composite and the convoluted spectra of individual element that are given in figure 7.

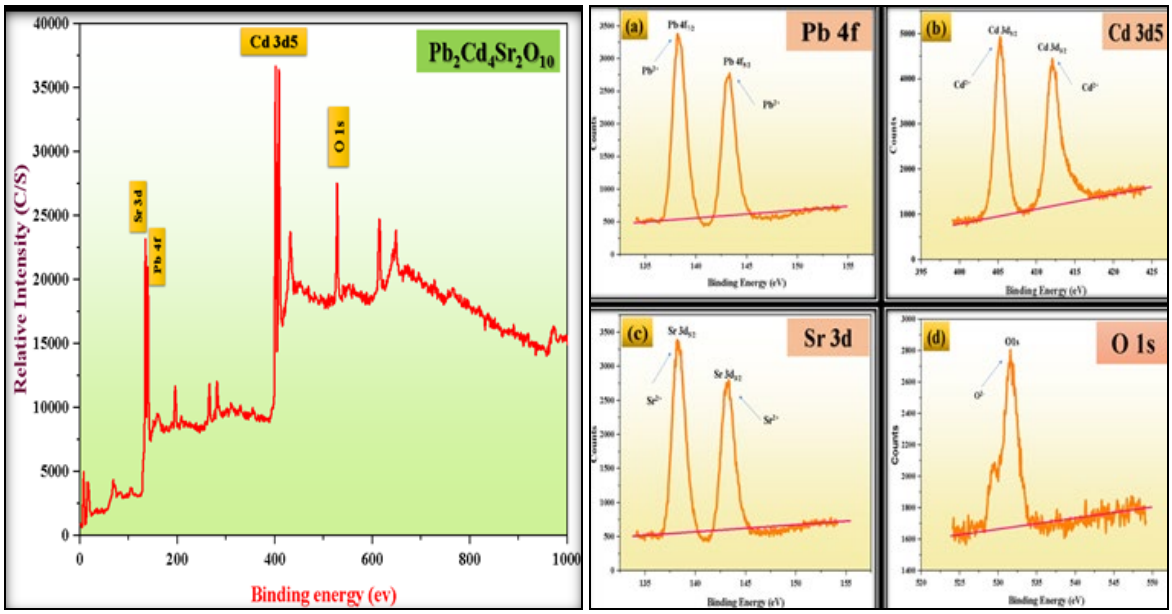

Fig 7: XPS analysis and convoluted spectra of individual elements

Observation of the peaks identifies that the photocatalyst comprises of Pb, Cd, Sr, and O elements. The binding energy for Pb in composite corresponds to Pb (II) 4f7/2 and 4f5/2 transitions located at 138.9 and 143.3 eV and is endorsed by Qi *et al.*[32] The binding energy for Cd in the composite corresponds to Cd (II) 3d5/2 and 3d3/2 transitions with a binding energy of 405.3 and 412.1 eV. [33] Binding energy located at 134.8 and 142.3 eV corresponds to the peaks for Sr (II) 3d5/2 and 3d3/2 transitions. [34, 35]. The binding energy for major peak O1s is found to be located at 531.5 eV which can be attributed to the presence of bound oxygen on the surface of nanocrystals.

3.7. FTIR Analysis

FTIR analysis is carried out in the 400-4000 cm^{-1} frequency range and the resulting spectra is given in figure 8.

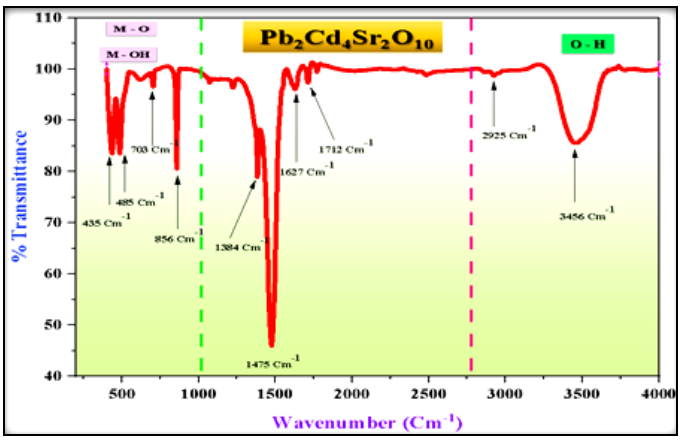

Fig 8: FT-IR spectra of $Pb_2Cd_4Sr_2O_{10}$ photocatalyst

The peaks at 3456 cm^{-1} and 1627 cm^{-1} are assigned to surface hydroxyl and adsorbed water molecules (O-H bending and stretching vibrations). The absorption peak at 485 cm^{-1} indicates the presence of Pb-O bond (PbO_2 stretching and bending vibrations).[36] The peaks observed at 703 and 856 cm^{-1} are indication of Cd-O bond (CdO stretching and bending vibrations).[37] The peak observed at 435 cm^{-1} corresponds to the asymmetric vibration of the Sr-O bond (SrO stretching and bending vibrations).[31] A shift in general peaks has been observed. All peaks were sharp stating the presence of strong stretching vibrations and denying the presence of impurities.

3.8. UV-VIS NIR Analysis

Figure 9 displays the UV-vis absorption spectra of $Pb_2Cd_4Sr_2O_{10}$.

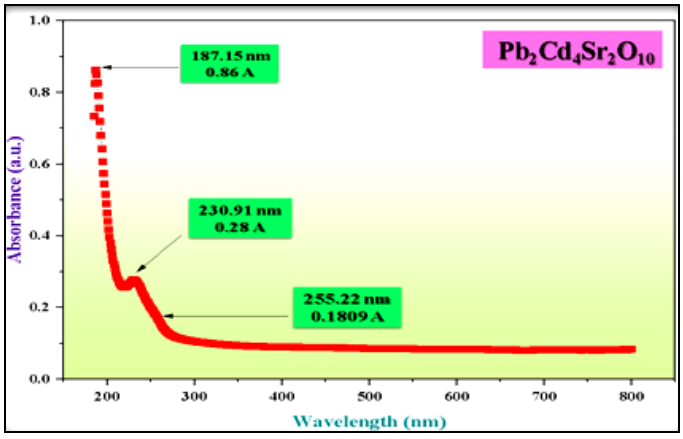

Fig 9: UV-VIS spectra of $Pb_2Cd_4Sr_2O_{10}$ photocatalyst

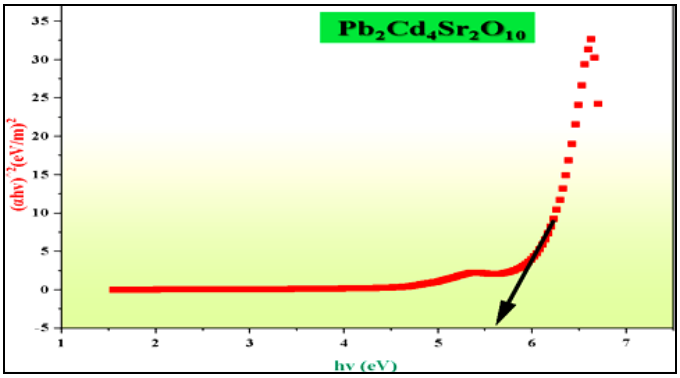

Fig 10: TAUC plot of Pb2Cd4Sr2O10 photocatalyst

A significant absorption in ultraviolet region is observed. [38] The peaks at 187 nm correspond to that of PbO_2, at 231 nm to SrO and in the range 250-300 nm for CdO. Because of the increased wavelength and less electron-hole recombination, the absorption of the nanocomposite is found to be greater than that of PbO-CdO nanocomposites. Tauc function is typically used to estimate the optical bandgap using experimental absorbance data and is calculated for $Pb_2Cd_4Sr_2O_{10}$ by Equation:

$$(\alpha h\nu)^2 = k\,(h\nu - E_g) \qquad (2)$$

Where hν stands for photoenergy, Eg for band energy, k for constant value, and α for absorption constant. The bandgap energy obtained through calculation is 5.6 eV (Figure 10). The interaction of PbO_2 and CdO with the SrO phase is found responsible for it. The large values of Eg (5.6 eV) of the prepared composite which belong to the ultraviolet range enables their usage in other applications such as energy storage applications, increase in the photocatalytic performance etc. When assisted by UV-vis irradiation

4. Kinetic Study of Degradation of Erythrosine B

The prepared photocatalyst was used for degradation of color pollutants in water. For this erythrosine B was selected as role model. Figure 11 shows the typical run.

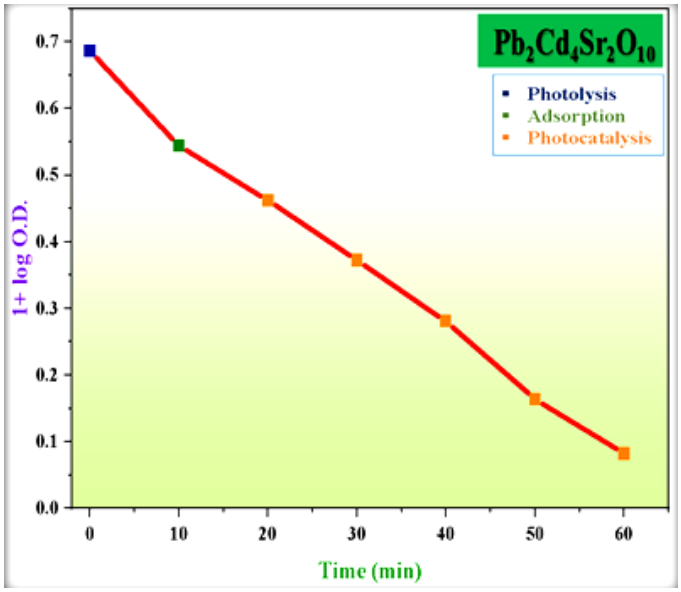

Fig 11: A typical run

It was observed through various studies that the reaction follows pseudo first order kinetics law. Different factors pH, concentration of dye, amount of photocatalyst and intensity of light were varied to extract maximum degradation conditions. The data are summarized in table 2. The dye degrades up to 98.76% in 60 minutes of exposure to light with value of rate constant 4.007 x 10^{-4} (sec^{-1}) at pH = 6.5, Dye concentration = 0.6 x 10^{-5} M, amount of photocatalyst = 0.1g and intensity of light= 1530 mW/cm^2.

Table 2: Rate constants at different variable conditions

pH	Rate Constant k x 10^{-4} (sec^{-1})	Concentration of dye x 10^{-4} (Moles/Litre)	Rate Constant k x 10^{-4} (sec^{-1})	Amount of photocatalyst(g)	Rate Constant k x 10^{-4} (sec^{-1})	Intensity of light (mW/cm^2)	Rate Constant k x 10^{-4} (sec^{-})
4.0	2.656	0.4	3.966	0.04	1.734	1530	4.007
5.0	3.204	0.6	4.007	0.06	1.794	1160	0.233
5.5	3.936	0.8	2.833	0.08	1.674	865	0.149
6.0	3.204	1.0	2.563	0.10	4.007	560	0.089
6.5	4.007	1.2	3.372	0.12	1.333		
7.0	3.753	1.4	1.618	0.14	1.489		
7.5	3.500	1.6	1.484	0.16	1.614		
8.0	3.753	1.8	0.944	0.18	1.489		
8.5	2.530			0.20	1.453		
9.0	2.403			0.22	1.674		

Scavenger study is carried out and it is observed that the reaction ceases completely on addition of isopropyl alcohol suggesting the participation of $OH^{\bullet}$ free radical as active species responsible for complete degradation of the dye. The end products are confirmed through laboratory tests. It is also observed that the photocatalyst works at same efficiency up to five cycles when is calcined and reused. A mechanism of degradation is proposed here by:

$Pb_2Cd_4Sr_2O_{10} + h\upsilon \rightarrow Pb_2Cd_4Sr_2O_{10}\ (e^-) + Pb_2Cd_4Sr_2O_{10}\ (h^+)$ (3)

$h^+ + OH^- \rightarrow OH^{\bullet}$ (4)

$e^- + O_2 \rightarrow O_2^{\bullet -}$ (5)

$H_2O + O_2^{\bullet -} \rightarrow HOO^{\bullet} + OH^{\bullet}$ (6)

$HOO^{\bullet} + h^+ \rightarrow H_2O_2$ (7)

$H_2O_2 + e^- \rightarrow OH^{\bullet} + OH^{-\bullet}$ (8)

$Dye + OH^{\bullet} \rightarrow CO_2 + H_2O$ (9)

5. Conclusions

The study leads to the conclusion that a novel photocatalyst $Pb_2Cd_4Sr_2O_{10}$ nanoparticles are synthesized. Various analytical methods are used to characterize it. The optical bandgap, Eg is calculated to 5.6 eV and the particle size calculated to be 46.96 nm with a nanosheet shape. It is then used for photocatalytic degradation of erythrosine B dye. When exposed to visible light, the nanocomposite demonstrates excellent photoactivity and after 60 minutes, nearly 99 percent degradation is observed. The values of k fits exactly to the pseudo-first-order rate equation. Even after five cycles, the photocatalyst photodegradation efficiency of over 90% is maintained, indicating its high stability and reusability. It is observed that $OH^{\bullet}$ is the active species causing the degradation. A mechanism is also proposed. Numerous possible uses for the produced materials are anticipated, such as solar cells, photocatalytic hydrogen evolution, and water splitting, photocatalytic degradation of organic matter etc.

References

1. Yang J, Wang D, Han H, Li CAN. Roles of cocatalysts in photocatalysis and photoelectrocatalysis. Acc. Chem. Res., 2013; 46(8):1900-1909. https://doi.org/10.1021/ar300227e
2. Xu C, Anusuyadevi PR, Aymonier C, Luque R, Marre S. Nanostructured materials for photocatalysis. Chem. Soc. Rev., 2019; 48(14):3868-3902. https://doi.org/10.1039/C9CS00102F
3. Nakata, K., Fujishima A. TiO_2 photocatalysis: Design and applications. *J. photochem. Photobiol. C: Photochem. Rev.,* 2012: 13(3): 169-189. https://doi.org/10.1016/j.jphotochemrev.2012.06.001
4. Wenderich K, Mul G. Methods, mechanism, and applications of photo deposition in photocatalysis: a review. Chem. Rev. 2016: 116(23):14587-14619. https://doi.org/10.1021/acs.chemrev.6b00327
5. Kumar R, Anandan S, Hembram K, Narasinga Rao T. Efficient ZnO-based visible-light-driven photocatalyst for antibacterial applications. Acs app. Mat. Interfaces. 2014; 6(15):13138-13148. https://doi.org/10.1021/am502915v
6. Xie J, Wang H, Duan M, Zhang L. Synthesis and photocatalysis properties of ZnO structures with different morphologies via hydrothermal method. App. Sur. Sci., 2011; 257(15):6358-6363. https://doi.org/10.1016/j.apsusc.2011.01.105
7. Kiriakidis G, Binas V. Metal oxide semiconductors as visible light photocatalysts. *J. Korean Phy. Soc*., 2014; 65:297-302.
8. Wang K, Wu X, Wu W, Chen W, Qin L, Cui W. Synthesis of rambutan-like $MnCo_2O_4$ and its adsorption performance for methyl orange. J. Therm. Analysis Calorimetry. 2015; 122:653-663.
9. Wu W, Liang S, Wang X, Bi J, Liu P, Wu L. Synthesis, structures, and photocatalytic activities of microcrystalline $Abi_2Nb_2O_9$ (A= Sr, Ba) powders. *J. Solid-State Chem*., 2011; 184(1):81-88.
10. Dineshbabu N, Jayaprakash RN, Karuppasamy P, Arun T, Vijaya JJ, Nimshi RE, Ramasamy P. Investigation on Tetracycline degradation and bactericidal properties of binary and ternary ZnO/NiO/g-C_3N_4 composites prepared by a facile coprecipitation method. *J. Environ. Chem. Eng.* 2022; 10(3):107368.
11. Elhalil A, Elmoubarki R, Farnane M, Machrouhi A, Mahjoubi FZ, Sadiq M, Barka N. Novel Ag-ZnO-$La_2O_2CO_3$ photocatalysts derived from the Layered Double Hydroxide structure with excellent photocatalytic performance for the degradation of pharmaceutical compounds. *J. Sci.: Adv. Mat. Devices*, 2019; 4(1):34-46.
12. Zhang D, Cui S, Yang J. Preparation of Ag_2O/g-C_3N_4/Fe_3O_4 composites and the application in the photocatalytic degradation of Rhodamine B under visible light. *J. Alloys Comp.,* 2017; 708:1141-1149.
13. Taddesse AM, Alemu M, Kebede T. Enhanced photocatalytic activity of pn heterojunctions ternary composite $Cu_2O/ZnO/Ag_3PO_4$ under visible light irradiation. *J. Env. Chem. Eng*., 2020; 8(5):104356.
14. Marsooli MA, Nasrabadi MR, Fasihi-Ramandi M, Adib K, Eghbali M, Pourmasoud S, Ganjali MR. Preparation of $Fe_3O_4/SiO_2/TiO_2/PrVO_4$ nanocomposite in various molar ratios: Investigation on photocatalytic performance on organic contaminate and bacterial environments, and anti-cancer properties. Polyhedron. 2020; 176:114239.
15. Muneer I, Farrukh MA, Ali D, Bashir F. Heterogeneous photocatalytic degradation of organic dyes by highly efficient $GdCoSnO_3$. Mat. Sci. Eng.: B, 2021; 265:115028.
16. Marzougui B, Smida YB, Marzouki R, Onwudiwe DC, Al-Douri Y, Hamzaoui AH. Combustion synthesis, characterization, and photodegradation performance of La_2-xBi_xCuO_4. Solid State Commun. 2023; 364:115113.
17. Sabzehmeidani MM, Karimi H, Ghaedi M. Nanofibers-based quaternary CeO_2/Co_3O_4/Ag/Ag_3PO_4 S-scheme heterojunction photocatalyst with enhanced degradation of organic dyes. Mat. Res. Bull. 2022; 147:111629.
18. Nihalani S, Vijay A, Bhardwaj S. Use of a new nanosized photocatalyst $BaO_3TiO.SrO_3TiO$ for degradation of Azure B: An eco-friendly process. Arch. App. Sci. Res., 2013; 5 (6):103-108.
19. Oppong SO, Anku WW, Shukla SK, Govender PP. Synthesis and characterization of neodymium doped-zinc oxide-graphene oxide nanocomposite as a highly efficient photocatalyst for enhanced degradation of indigo carmine in water under simulated solar light. Res. Chem. Int., 2017; 43(1):481-501.
20. Nkambule TI, Kuvarega AT, Krause RWM, Haarhoff J, Mamba B.B. Synthesis and characterization of Pd-modified N-doped TiO_2 for photocatalytic degradation of natural organic matter (NOM) fractions. Environ. Sci. Poll. Res. 2012; 19(9):4120-4132.

21. Haw C, Chiu W, Rahman SA, Khiew P, Radiman S, Shukor S.A., Ghazali N. The design of new magnetic-photocatalyst nanocomposites ($CoFe_2O_4$-TiO_2) as smart nanomaterials for recyclable-photocatalysis applications. *New J. Chem*., 2016; 40(2):1124-1136.
22. Moradnia F, Taghavi Fardood S, Ramazani A, Osali S, Abdolmaleki I. Green sol-gel synthesis of $CoMnCrO_4$ spinel nanoparticles and their photocatalytic application. Micro Nano Lett. 2020; 15(10):674-677.
23. Oh WC, Fatema KN, Liu Y, Lim CS, Cho KY, Jung CH, Biswas MRUD. Sonochemical synthesis of quaternary $LaNiSbWO_4$-G-PANI polymer nanocomposite for photocatalytic degradation of Safranin-O and gallic acid under visible light irradiation. *J. Photochem. Photobiol. A: Chem*., 2020; 394:112484.
24. Otgonbayar Z, Liu Y, Cho KY, Jung CH, Oh WC. Novel ternary composite of $LaYAgO_4$ and TiO_2 united with graphene and its complement: Photocatalytic performance of CO_2 reduction into methanol. Mat. Sci. Semicond. Process, 2021; 121:105456.
25. Weller T, Sann J, Marschall R. Pore structure controlling the activity of mesoporous crystalline $CsTaWO_6$ for photocatalytic hydrogen generation. Adv. En. Mat., 2016; 6(16):1600208.
26. Chen Q, Wang Y, Wang H. Synthesis and properties of nanocrystal $BiPO_4$ in diamagnetic PbO-Bi_2O_3-B_2O_3 glass. *J. Non-Crystalline Solids*, 2018; 481:85-93.
27. Babaahamdi-Milani M, Nezamzadeh-Ejhieh A. A comprehensive study on photocatalytic activity of supported Ni/Pb sulfide and oxide systems onto natural zeolite nanoparticles. *J. Haz. Mat*., 2016; 318:291-301.
28. Munawar T, Yasmeen S, Hussain F, Mahmood K, Hussain A, Asghar M, Iqbal F. Synthesis of novel heterostructured ZnO-CdO-CuO nanocomposite: characterization and enhanced sunlight driven photocatalytic activity. Mat. Chem. Phy., 2020; 249:122983.
29. Naeem R, Yahya R, Pandikumar A, Ming HN, Mazhar M. Optical and optoelectronic properties of morphology and structure controlled ZnO, CdO and PbO thin films deposited by electric field directed aerosol assisted CVD. *Journal of Materials Science: Mat. Electron.* 2017; 28:868-877.
30. Chen H, Xu X. Ruddlesden-Popper compounds in the double-perovskite family Sr_2FeTaO_6 (SrO) n (n= 0, 1 and 2) and their photocatalytic properties. App. Catal. B: Environ. 2017; 206:35-43.
31. Subhan MA, Rifat TP, Saha PC, Alam MM, Asiri AM, Rahman MM, Uddin J. Enhanced visible light-mediated photocatalysis, antibacterial functions, and fabrication of a 3-chlorophenol sensor based on ternary $Ag_2O{\cdot}SrO{\cdot}CaO$. RSC adv., 2020; 10(19):11274-11291.
32. Qi X, Xie F. Promotion effects of potassium permanganate on the removal of Pb (II), Ni (II), and Cd (II) from hydrous manganese dioxide. *Chem. Eng. J.,* 2018; 351:22-30.
33. Rahman MM, Khan SB, Marwani HM, Asiri AM, Alamry KA, Rub MA, Azum N. Facile synthesis of doped ZnO-CdO nano blocks as solid-phase adsorbent and efficient solar photo-catalyst applications. *J. Ind. Eng. Chem.* 2014; 20(4):2278-2286
34. Prakash K, Senthil KP, Latha P, Shanmugam R, Karuthapandian S. Dry synthesis of water lily flower-like SrO_2/g-C_3N_4 nanohybrids for the visible-light-induced superior photocatalytic activity. Mat. Res. Bull. 2017; 93:112-122.
35. Kılıç D, Sevim M, Eroğlu Z, Metin Ö, Karaca S. Strontium oxide modified mesoporous graphitic carbon nitride/titanium dioxide nanocomposites (SrOmpg-CN/TiO_2) as efficient heterojunction photocatalysts for the degradation of tetracycline in water. Adv. Powder Technol. 2021; 32(8):2743-2757.
36. Shifu C, Sujuan Z, Wei L, Wei Z. Preparation and activity evaluation of p-n junction photocatalyst NiO/TiO_2. J. Hazar. Mat., 2008; 155(1-2):320-326.
37. Abu-Dief AM, Essawy AA, Diab AK, Mohamed WS. Facile synthesis and characterization of novel Gd_2O_3-CdO binary mixed oxide nanocomposites of highly photocatalytic activity for wastewater remediation under solar illumination. *J. Phy. Chem. Solids*, 2021; 148:109666.
38. Lohar S, Vijay A, Bhardwaj S. Visible light-driven degradation of xanthene dyes using novel synthesized quaternary nanomaterial $ZrCdPbO_4$. *Inter. J. Env. Anal. Chem*. 2023; 103(16):4876-4889. https://doi.org/10.1080/03067319.2021.1931858